SPE 166374

Experimental Study of Liquid Viscosity Effect on Two-Phase Stage Performance of Electrical Submersible Pumps

H. M. Banjar, SPE, J. Gamboa, SPE, and H.-Q. Zhang, SPE, University of Tulsa

This paper was prepared for presentation at the SPE Annual Technical Conference and Exhibition held in New Orleans, Louisiana, USA, 30 September–2 October 2013.

Abstract

Experiments with a seven-stage Electrical Submersible Pump (ESP) have been carried out to study the effect of liquid viscosity on the gas-liquid two-phase stage performance. The experimental tests provided data about the stage pressure increment as a function of the liquid flow rate at constant rotational speed, inlet pressure, and volumetric gas flow rate. Two different mineral oils were used so that the ESP two-phase stage performance was measured for 1 cP, 1.2 cP and 8.5 cP liquid viscosities, and for 8 different gas flow rates.

The experimental results demonstrate that the increase of liquid viscosity causes gas surging in the stage to initiate at lower normalized gas flow rates, reducing the gas handling capability of the stage. Increasing the liquid viscosity also causes the stage to reach a zero pressure increment at a higher normalized liquid flow rate. The pressure increment deterioration caused by the gas worsens with increased liquid viscosity. The performance map is analyzed and compared with that of another pump (GC-6100) with a higher inlet stage pressure.

Introduction

Oil reservoir pressure decreases with production, especially when no pressure maintenance methods, such as water injection, are used. Sometimes the pressure in a well is high enough to produce naturally, but higher oil production is required in order to maximize the oil recovery and to reduce the investment return time. Artificial lift methods are used to help overcome pressure losses in such wells in order to maintain or increase production rates. ESP provided artificial lift for about 14% of the world's wells during 2000 (Prado 2011).

ESPs are suitable for wells that have an intermediate range of temperature, no sand, and no gas production. However, it is not unusual for some of these wells to have free gas which deteriorates ESP performance and efficiency.ESP performance is affected by many factors including rotational speed, bubble size, fluid density and viscosity. The effects of these variables on pump performance need to be investigated and prediction models need to be developed. Although correlations and models for predicting the effects of some of these variables have been formulated, most of them have been only partially validated. Moreover, the physical mechanism that governs the ESP performance under gassy condition is not fully understood. Therefore, the development of mechanistic models has been hindered. This study intends to improve understanding of ESP performance at different liquid viscosities and Gas Volumetric Fractions (GVF).

Most of the research about the two-phase ESP performance has been carried out with water and air. There were a few studies that investigate the effect of viscosity on the ESP performance, but none of these studies dealt with the combined effects of gas fraction and liquid viscosity on ESP performance. The objective of this work is to gather experimental data to show the effect of liquid viscosity on the two-phase performance of an ESP stage.

Flowloop Layout

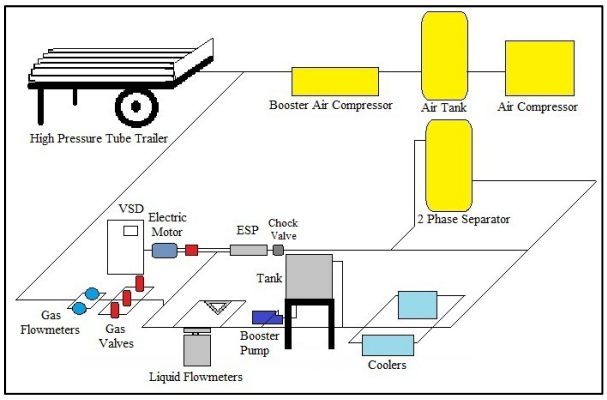

Fig. 1: Schematic Diagram of Two-Phase Flow Loop

Fig. 1 shows the layout of the facility utilized in this study. The ESP tested is a seven-stage mixed flow type pump DN-1750. The pump is hooked up to a thrust chamber that holds the pump thrust and allows the shaft to rotate. The pump is driven by a 100 hp AC electric motor that is controlled via a VSD.

Differential pressure is measured between the stage 3 outlet and the stage 4 inlet for stage performance, while absolute pressure and temperature gauges are located at the stage 3 outlet to calculate the GVF at the stage inlet. Differential pressure and temperature transducers are also installed between the stage 1 inlet and the stage 7 discharge to measure the ESP's overall performance. There are pressure and temperature transducers located downstream of the choke, at the ESP inlet pipeline and at the tank for process control purposes. A torque cell on the pump shaft measures the ESP torque and rotational speed.

Oil Used

Among the 10 Isoparaffinic fluid grades available, two oils were selected: Isoparaffinic fluid G and Isoparaffinic fluid V. The selections of these mineral oils are based on their viscosity range, from 0.855 cP to 20 cP. The latter is the maximum liquid viscosity for an efficient gas and liquid separation at the separator. The manufacturer provides information about the density at 60°F and kinematic viscosities at 40°C and 100°C for both oils. However, the manufacturer does not provide any information about the relationship between density and temperature. Therefore, a series of tests has been conducted in order to determine viscosity and density as a function of temperature for each of the mineral oils selected.

The viscosity as function of temperature is measured for both mineral oils. Then, the coefficients of Vogel's viscosity correlation, recommended by Stachowiak and Batchelor (2005) (Eq. 1), are determined for each oil. These coefficients are calculated by using the multiple regressions of the viscosity data using SOLVER function from Excel®. The viscosity measured and the viscosity calculated by Eq. 1 are presented in Fig. 2.

$$\mu = A \exp\left[\frac{B}{T + 460 + C}\right] \qquad \text{..... (1)}$$

where μ is the fluid viscosity in cP and T is the temperature in °F.

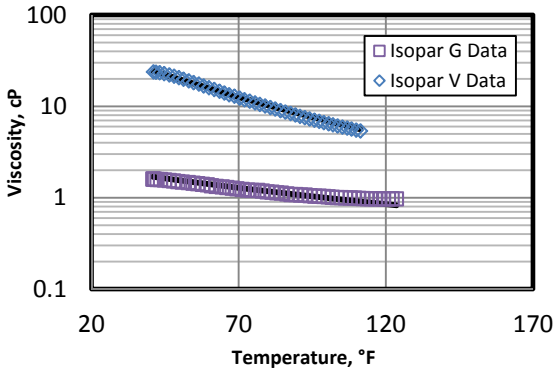

Fig. 2: Isoparaffinic Fluid G and Isoparaffinic Fluid V Viscosities vs. Temperature

The densities of the selected oils are measured at several different temperatures. Hydrometers calibrated at different temperatures are utilized in these measurements. The results of these measurements are presented in Fig. 3. For the thermal expansion of oil, Eq. 2 is used:

$$\rho = \rho_0 \exp^{\xi(T_0 - 0.5556T - 255.37)} \quad \text{..... (2)}$$

where ρ is the fluid density in g/ml and T is the temperature in °F.

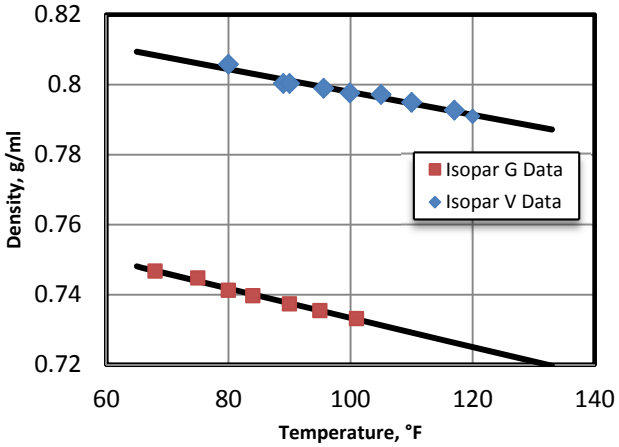

Fig. 3: Isoparaffinic Fluid G and Isoparaffinic Fluid V Densities vs. Temperature

Eq. 1 and Eq. 2 are used for experimental control. Since the viscosity and density of the fluid cannot be measured directly at the stage inlet, the stage inlet temperature is measured, and both the viscosity and density are calculated using Eq. 1 and Eq. 2.

Experiment Procedure

Zapata (2007) introduced a dimensionless factor for scaling the gas flow rate at different rotational speeds, which is known as the normalized gas flow rate. The normalized gas flow rate, q_{gd} , is defined as

$$q_{gd} = \frac{q_g}{q_{max}} \quad \text{..... (3)}$$

where q_g is the volumetric gas flow rate at stage intake pressure and temperature, and $q_{\max}$ is the single-phase open flow rate at a given rotational speed. The units of q_g and $q_{\max}$ must be consistent in order to get a dimensionless number q_{gd} . Eq. 3 is used to determine the volumetric gas flow rate at a given rotational speed by varying the normalized gas flow rate for a constant open flow rate (open flow rate is a function of the rotational speed with water).

Solano (2009) and Trevisan (2009) demonstrated that the open flow rate is also dependent on liquid viscosity if other fluids are used. However, the experimental matrix is based on the normalized gas flow rate as given in Eq. 3 in which $q_{\max}$ is defined as the zero-head flow rate at a given viscosity and rotational speed. In these experiments, the normalized gas flow rate does not exceed 15% in order to avoid a premature failure of the ESP due to excessive gas handling. The normalized gas flow rate is increased by 2% steps from the single-phase condition (zero normalized gas flow rate) up to 12%. Then, it is increased to 15% because major changes in the two-phase performance are not expected above 15% as observed by Gamboa (2009).

The rotational speed in these experiments is kept constant at 1,800 rpm. This value is chosen based on the results obtained from the single-phase test, in which the open flow rate (zero head) could not be achieved for rotational speeds higher than 2,000 rpm due to the booster pump capacity limitation.

The stage inlet pressure is held constant at 40 psig in these tests. Although this is quite low compared to the pressures utilized in other tests (Zapata 2007, Duran 2009 and Gamboa 2009), this is the maximum inlet pressure that could be controlled with the booster pump during the exploratory tests.

Naseri et al. (2005) reported that the crude oil under-saturated live viscosity ranges between 0.15 cP and 315 cP worldwide, while Sutton and Farshad (1990) mentioned that the live oil viscosity of Gulf of Mexico (GOM) crude oils ranges from 0.144 cP to 3.45 cP. Based on this information, three viscosity values have been chosen to be 1, 1.2 and 8.5 cP. The first viscosity value is 1 cP, which is utilized as the reference or baseline case. The other two viscosity values, 1.2 cP and 8.5 cP, are chosen because they cover the high viscosity end for GOM oils. These viscosity values may only cover the low viscosity range for worldwide oils.

Results and Discussions

Single-Phase Tests

Single-phase test results are presented in graphs with explanations. Single-phase test procedure is run from open flow rate towards the shut-in head.

Base Performance

Based on API RP 11S2, the base performance curve of an ESP is obtained with water. However, ESPs are used to pump oil in petroleum production. Also, use of water in the facility may cause corrosion and emulsion problems. The alternative is to use an oil with viscosity similar to water viscosity. After a search of commercial mineral lube oils, Isoparaffinic fluid G is chosen for obtaining the base stage performance curve at 98 °F. The test results at di°ferent rotational speeds are presented in Fig. 4.

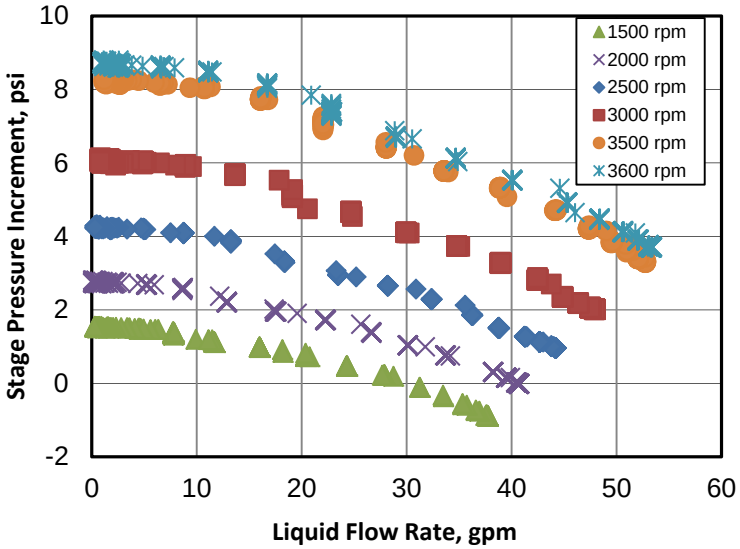

Fig. 4: Base Performance at 1 cP

The tests with Isoparaffinic fluid G are conducted at temperatures ranging from 57 °F to 73 °F at the stage inlet and the corresponding viscosities range between 1.25 cP and 1.45 cP. The density of this oil is lower than water density and ranges between 0.745 and 0.751 g/ml. Therefore, the pressure increment of the stage is lower than that reported by the manufacturer for water. Stepanoff (1957) stated that the stage performance is independent on the fluid properties as long it is expressed as head. Thus, the following equation is used to calculate the head generated by the stage.

$$H = \frac{\Delta p}{0.433\gamma_l} \quad \text{..... (4)}$$

where γ_l is the liquid specific gravity and H is the head in ft.

The head stage performance curves are then shown in Fig. 5 for three rotational speeds: 3,500 rpm, 2,400 rpm and 1,500 rpm. The performance curve from the manufacturer catalog at 3,500 rpm is also presented in Fig. 5, while the performance at other rotational speeds is obtained by applying the affinity law using the 3,500 rpm performance curve. Notice the difference between the experimental performance and the manufacturer performance is about 5 ft at the shut-in head at 3,500 rpm.

Affinity laws relate the ESP's rotational speed to the pump's flow rate, head developed by the ESP and break horsepower required to drive the pump. These laws are expressed as follows:

$$\frac{q_1}{q_2} = \frac{N_1}{N_2} \quad \text{..... (5)}$$

$$\frac{H_1}{H_2} = \left(\frac{N_1}{N_2}\right)^2 \quad \text{..... (6)}$$

$$\frac{BHP_1}{BHP_2} = \left(\frac{N_1}{N_2}\right)^3 \quad \text{..... (7)}$$

where q is the pump flow rate, H is the head developed by the pump and BHP is the break horsepower needed to drive the pump. Each parameter corresponds to the ESP's rotational speed, N.

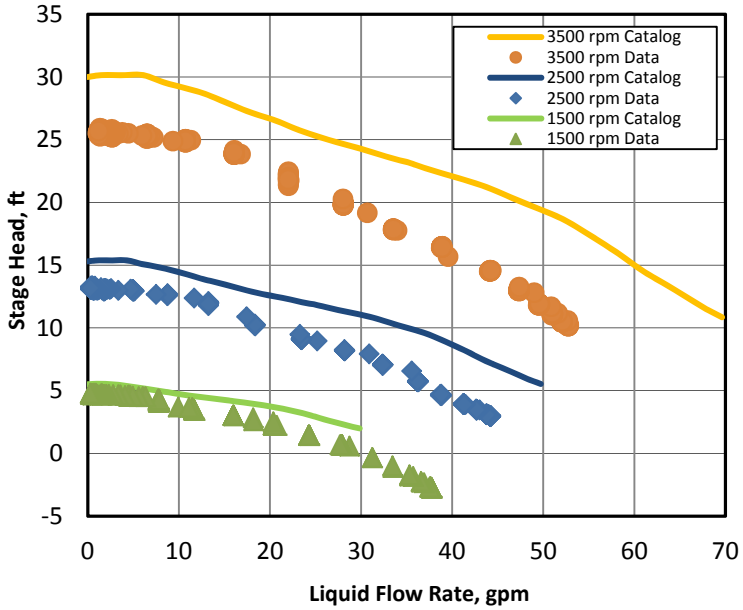

Fig. 5: Experimental and Manufacturer Performance Curves for DN-1750

The reason for this discrepancy is not very clear. It may be due to the fact that the manufacturer performance is obtained as the average stage performance (dividing the overall head of the pump by the number of stages). However, the comparison with the water performance presented by Solano (2009) also showed a similar discrepancy. Another possibility is there might be some mechanical problems with the stage. Despite of the deviation, the experimental performance is used as the base in this study.

Viscosity Effect

Fig. 6 presents the head performance curves at 1,800 rpm for liquid viscosity values of 1 cP, 1.2 cP and 8.5 cP. Note that the performance curve at 1.2 cP shows a higher head than that observed at 1 cP for the same flow rates. Li (2000) observed this head rising phenomenon in a volute-type centrifugal pump. The author explained that the head rising is due to flow regime transition in the boundary layer on the blade surface. The fluid goes from hydraulically rough to smooth reducing the friction losses.

The head curve at 8.5 cP is below the head curve at 1 cP, which means that the stage head at this viscosity is lower than that at 1 cP for the same flow rate. The open-flow rate goes from 37 gpm at 1 cP down to 32 gpm at 8.5 cP. However, the shut-in heads seem to be the same at both viscosities, which agrees with Hydraulic Institute standards (1955). Fig. 6 clearly shows that the head curve and the open flow rate are affected by the change of fluid viscosity.

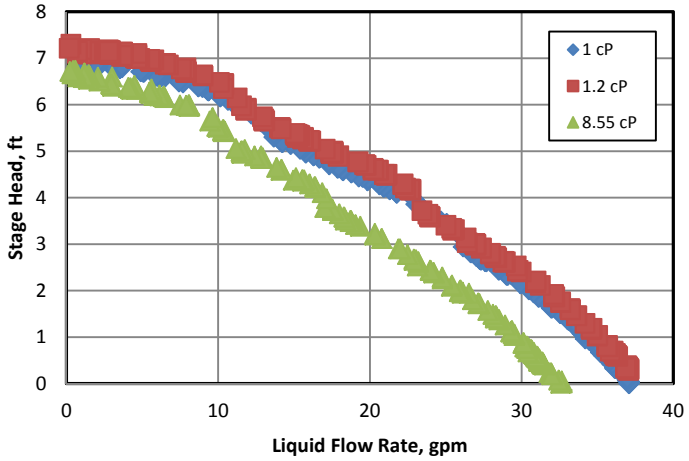

Fig. 6: Single-Phase Performance at Different Viscosities

Two-Phase Tests

A two-phase test procedure is run from open flow rate towards the shut-in head, keeping the gas mass flow rate constant as mentioned earlier.

Two-Phase Performance at 1 cP

The two-phase performance at 1 cP is presented in Fig. 7 for different normalized gas flow rates at 1,800 rpm. It is observed that the performance curve at 2% normalized gas flow rate overlaps the single-phase performance implying that the stage performance is not affected by the gas at this low normalized gas flow rate.

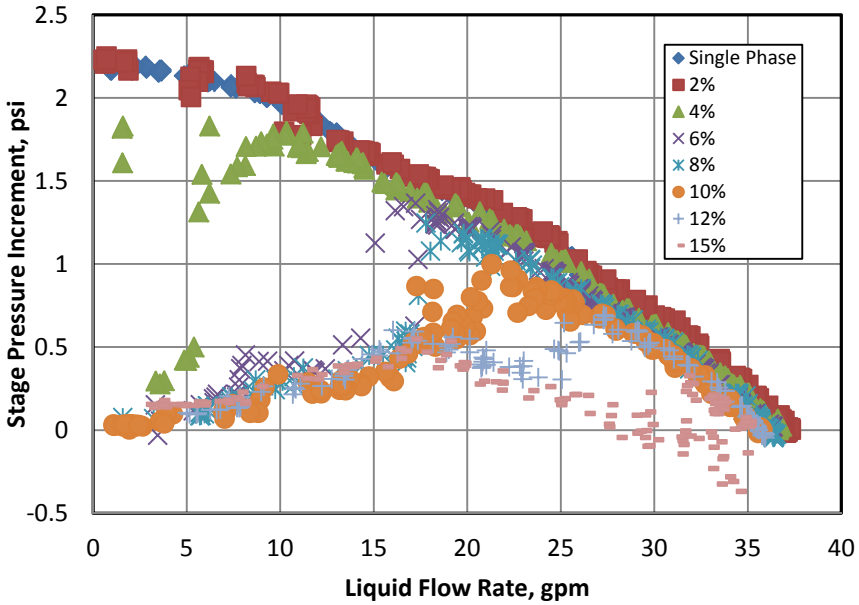

Fig. 7: Two-Phase Performance at 1 cP and Different q_{gd}

Fig. 7 shows that there is a critical liquid flow rate in every performance curve above 2% normalized gas flow rate that marks the beginning of the scattering in the experimental data and a sudden drop of the head. This liquid flow rate also corresponds to the maximum pressure increment generated by the stage. This behavior meets the criterion for surging initiation given by Gamboa (2009). The surging in the stage initiates at higher liquid flow rate as the normalized gas flow rate is increased.

The stage pressure increment deterioration from the single-phase performance is small for normalized gas flow rates between 4% and 10% at liquid flow rates higher than the values corresponding to the surging initiation. However, the deterioration becomes severe at liquid flow rates lower than the surging initiation for these normalized gas flow rates. On the other hand, the pressure increments for 12% and 15% normalized gas flow rates are severely deteriorated even at liquid flow rates near open flow.

Two-Phase Performance at 1.2 cP

The two-phase stage performance observed at 1.2 cP (Fig. 8) is very similar to that depicted at 1 cP. However, the surging initiates at liquid flow rates slightly higher than those observed at 1 cP. For instance, at 10% normalized gas flow rate, the surging initiates at 22 gpm for 1 cP, while this condition occurs at 27 gpm for 1.2 cP. The surging initiation for 2% normalized gas flow rate could not be identified in the two-phase performance curve at 1 cP, while it is observed at about 3 gpm for 1.2 cP. Clearly, the viscosity increase has altered the liquid flow rate at which the surging initiates.

Again the surging initiation is marked by the beginning of the scatter in the experimental data and the sudden head drop. The two-phase performance before the surging initiation is like the single-phase performance (the pressure increment increases with the liquid flow rate reduction). The pressure increment deterioration is mild for normalized gas flow rates between 2% and 10% and it becomes severe for 12% and 15%.

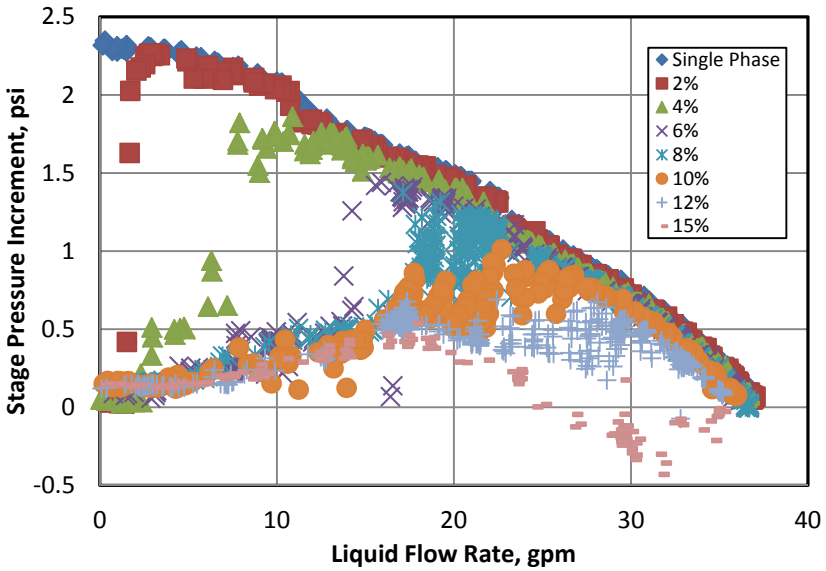

Fig. 8: Two-Phase Performance at 1.2 cP and Different q_{gd}

The two-phase performance after the surging initiation exhibits two different behaviors. A sudden pressure increment reduction is observed at the surging initiation. Then, the pressure increment reduces with the reduction of the liquid flow rate. The two-phase pressure increment for normalized gas flow rates between 6% and 15% follows a single trend at liquid flow rates between 15 gpm and 3 gpm. In this range, the pressure increment seems to mildly reduce with the reduction of liquid flow rate. At 3 gpm, the pressure increment becomes almost zero for all the normalized gas flow rates evaluated.

Two-Phase Performance at 8.5 cP

Fig. 9 shows the two-phase performance curves obtained at 8.5 cP for normalized gas flow rates between 0% and 15%. It is observed that the surging initiation occurs at higher liquid flow rates than the previous lower viscosity cases. The pressure increments at 2% and 4% normalized gas flow rates show a mild deterioration from the single-phase performance at liquid flow rates higher than 14 gpm and 22 gpm, respectively. Severe deterioration in the pressure increment is observed for all normalized gas flow rates above 6%. It implies that the severe deterioration has occurred at lower normalized gas flow rates than that observed for lower oil viscosities.

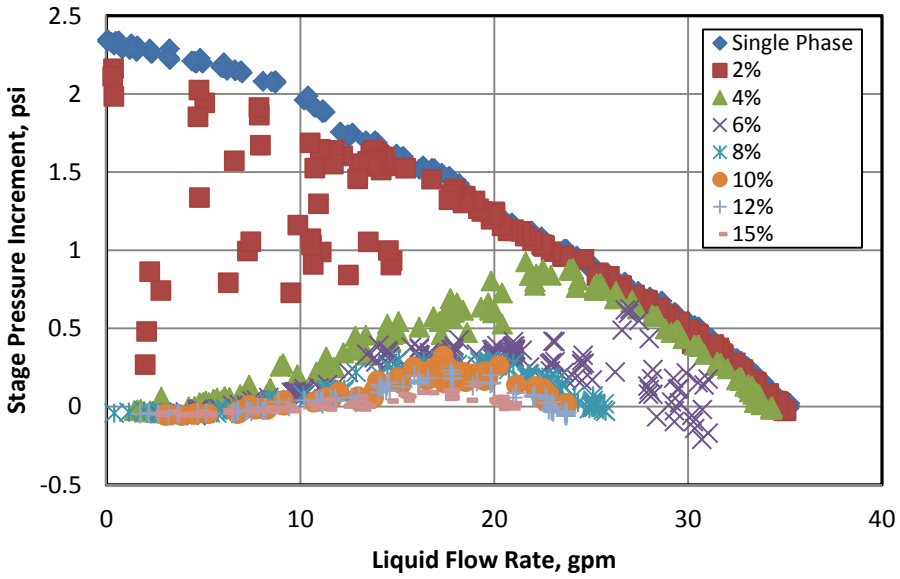

Fig. 9: Two-Phase Performance at 8.5 cP and Different q_{gd}

The severity of the pressure increment deterioration is such that the maximum pressure increment at 8.5 cP is slightly above 1 psi at 6% normalized gas flow rate when a maximum pressure increment of 4 psi is reached at 1 cP and 1.2 cP for the same normalized gas flow rate. Fig. 9 also shows that the pressure increment becomes almost zero at liquid flow rates smaller than 10 gpm. The pressure increment at 15% normalized gas flow rate is close to zero. The stage does not provide any pressure generation capability at this gas flow rate.

Analysis

Effect of Viscosity on Surging Initiation

The surging initiation is identified in this study utilizing two criteria:

1. The surging initiates at the liquid flow rate where the maximum pressure increment is observed.
2. The surging initiation occurs at the liquid flow rate where the scatter of the experimental data begins.

Based on these criteria, the surging initiation points are presented in Fig. 10.

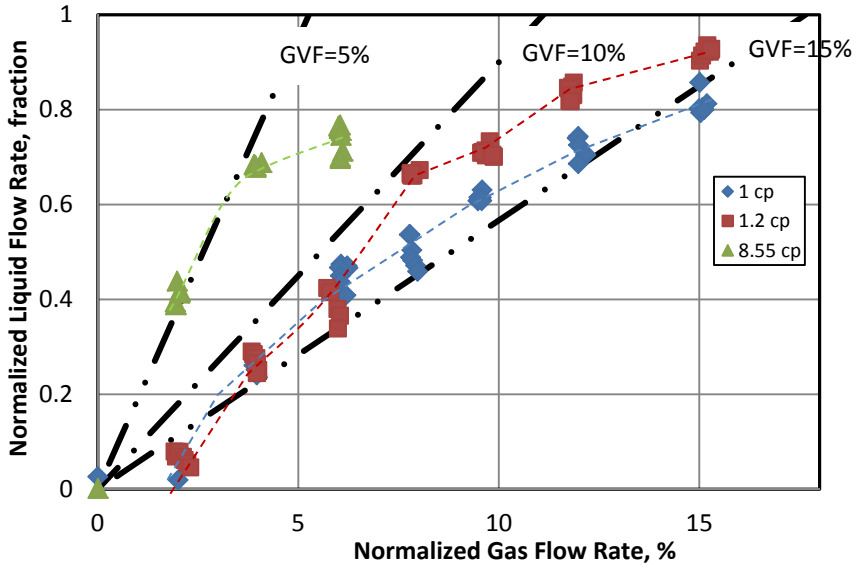

Fig. 10: Effect of Viscosity on Surging Initiation

Fig. 10 presents the normalized liquid flow rate at which the surging is identified for every normalized gas flow rate tested. Dashed lines are added to show the trend of the experimental data. Dashed-Dot lines are also included to indicate the

constant gas volumetric fractions (GVF) at 5%, 10% and 15%. GVF is calculated assuming gas and liquid flow at the same velocity.

$$GVF = \frac{q_g}{q_g + q_l} \quad \text{..... (8)}$$

Where q_g and q_l are the volumetric gas and liquid flow rates at stage intake pressure and temperature, respectively.

The comparison shows that the surging initiation does not occur at constant GVF instead this critical condition is a function of the liquid flow rate as mentioned by Gamboa (2009) as well as fluid properties. It is observed that the increase of the liquid viscosity causes the surging to initiate at lower GVF as stated by Trevisan (2009). Pump produces less head as a result of viscosity increase in two-phase operation.

Effect of Viscosity on Performance Map

Gamboa's (2009) performance map is used in this study for analyzing the viscosity effects on the behavior of the operating regimes of an ESP stage under two-phase conditions. Two transitions, the surging initiation and the open-flow were mapped, because these two transitions bracket a regime that encloses the operating conditions in which the stage is still performing under two-phase conditions. This operating regime is designated as mild deterioration regime following Gamboa's (2009) classification.

The transitions are identified based on the behavior of the pressure increment. Fig. 11 presents the performance map for the experimental data collected for liquid viscosity of 1 cP where the x-axis represents the normalized gas flow rate and the y-axis is the normalized liquid flow rate. The diamond symbols represent the open-flow boundary corresponding to the dividing point between pressure increment positive and negative. The square symbols are the surging initiation. The highlighted region in this figure encloses the mild deterioration regime.

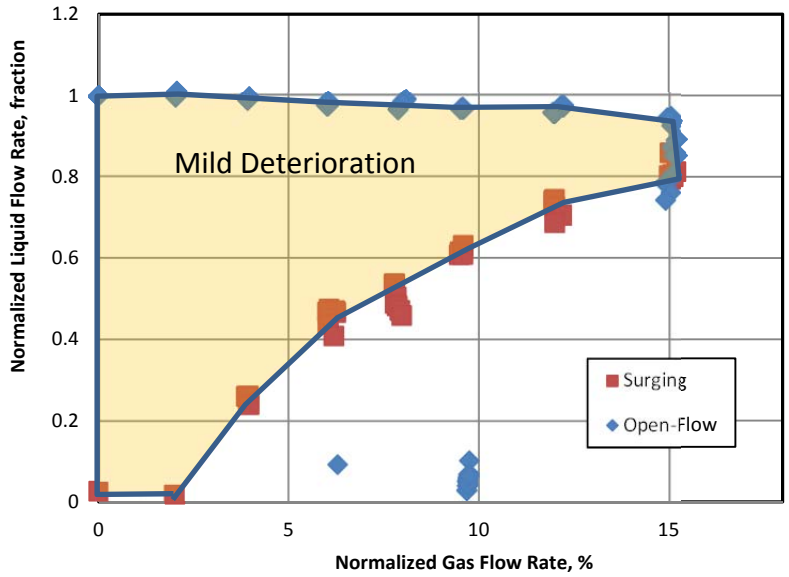

Fig. 11: Performance Map at 1 cP

It is observed that the open-flow boundary does not remain constant at 1; instead, it drops slightly with the increase of normalized gas flow rate. Gamboa (2009) explained that this phenomenon is mainly due to the gas presence which occupies part of the liquid volume. However, several normalized liquid flow rates satisfy the zero-head condition at 15% normalized gas flow rate. This condition may represent the maximum gas flow rate that the pump can handle at any liquid flow rate for the stage inlet pressure 38 psig.

The zero-head operating condition is also obtained at some experimental points that are observed in the lower part of Fig. 11. Since these points are located at liquid flow rates much lower than the open-flow boundary at 10% normalized gas flow rate, it is assumed that these points belong to the 3rd boundary mentioned by Gamboa (2009). This boundary sets the transition to the zero pump head. The experimental data actually shows three of the transitions observed by Gamboa (2009).

Fig. 12 presents the performance map obtained at oil viscosity 1.2 cP. It is seen that the mild deterioration regime has shrunk compared to the performance map at 1 cP. For instance, the stage generates pressure at normalized liquid flow rates between 0.98 and 0.75 for 12% normalized gas flow rate at 1 cP, while the same operating region is observed at normalized liquid flow rate between 0.95 and 0.82 at 1.2 cP liquid viscosity. However, this phenomenon is only observed at normalized liquid flow rates greater than 0.6. The mild deterioration regime at 1.2 cP coincides with the same regime at 1 cP for

normalized liquid flow rates lower or equal to 0.6. As occurred at 1 cP, the open-flow boundary meets the surging boundary at 15% normalized gas flow rate. This means that 15% is the maximum normalized gas flow rate above which the pump cannot generate pressure.

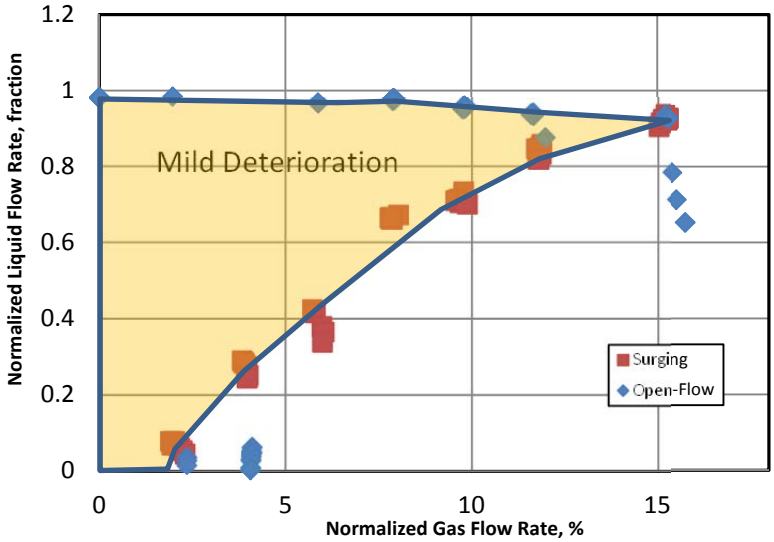

Fig. 12: Performance Map at 1.2 cP

Further increase of liquid viscosity up to 8.5 cP causes a drastic reduction of the mild deterioration regime as shown in Fig. 13. Notice that the open flow boundary quickly moves away from 1 at normalized gas flow rates as low as 4%. The open flow boundary moves to lower liquid flow rate as the normalized gas flow rate is increased indicating that gas reduces the liquid flow rate at which the stage stops generating pressure under two-phase conditions.

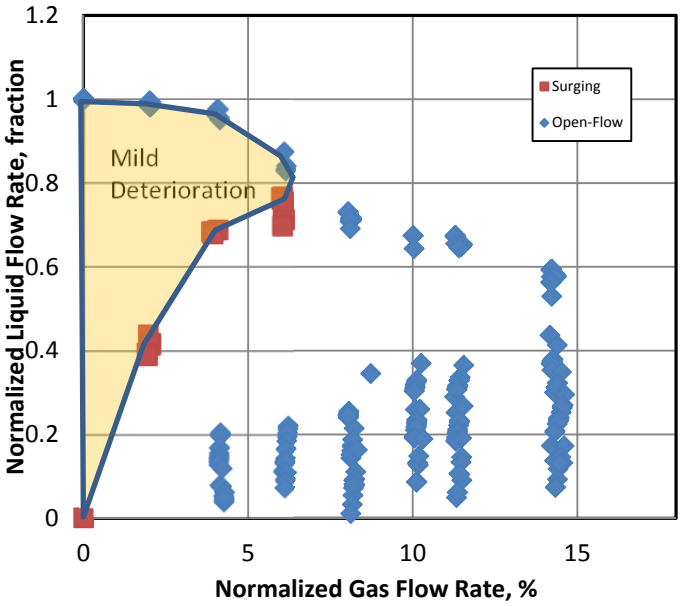

Fig. 13: Performance Map at 8.5 cP

The maximum normalized gas flow decreases to 6% at 8.5 cP compared to the 15% observed at lower viscosities. The nil pump head regime seems to expand so that it occurs at normalized liquid flow rates between 0.2 and 0.6. The performance presented in Fig. 13 demonstrates that the performance of the stage under two-phase conditions is dramatically affected by the liquid viscosity. The effect is observed in the surging initiation that occurs at lower normalized gas flow rates. This also occurs in the open flow boundary that moves to lower normalized liquid flow rates, and in the nil pump head regime that expands to higher normalized liquid flow rates.

Comparison between GC-6100 and DN-1750

Finally, the performance map obtained by Gamboa (2009) with ESP GC-6100 is compared to the map obtained in this study for ESP DN-1750 in Fig. 14. Note that both performance maps look alike even though boundaries or transitions occur at different normalized liquid and gas flow rates. The comparison seems to indicate that a DN-1750 ESP stage can handle more gas than a GC-6100 ESP stage even though the performance map for the latter ESP stage was acquired at higher stage inlet pressure. This observation clearly contradicts the well-known finding that the performance of any ESP improves with the increase of stage inlet pressure.

Based on the specific speed number, the GC-6100 stage is classified as highly mixed-type flow pump while the DN-1750 stage is more radial-type flow pump. Based on Lea and Bearden (1982) experimental results, mixed-type flow ESPs can handle more gas than radial-type flow ESPs. Consequently, the DN-1750 stage should handle less gas than the GC-6100 stage. However, the experimental results contradict this well-known heuristic rule. This result shows that the geometry classification based on specific speed is not a reliable parameter to define the two-phase performance of an ESP stage. These results lead to the hypothesis that there are other factors causing the improvement of gas handling in the DN-1750 ESP stage. For instance, this phenomenon may be attributed to the low surface tension of the oil used in the tests. While Gamboa (2009) used water (72 dyne/cm) in his experiments, the current experiments are carried out using lube oil with a surface tension about 33 dyne/cm. Based on Gamboa's (2009) observations, the reduction of surface tension causes a drastic reduction of the bubble size. As a result, the stage shows a better performance under gassy conditions. Thus, the improvement in the gas handling capability of the DN-1750 ESP stage may be due to the surface tension rather than the geometry. However, the current experimental data do not provide further insight about the causes of such a difference. Further research on the subject is required in order to understand the physical mechanism.

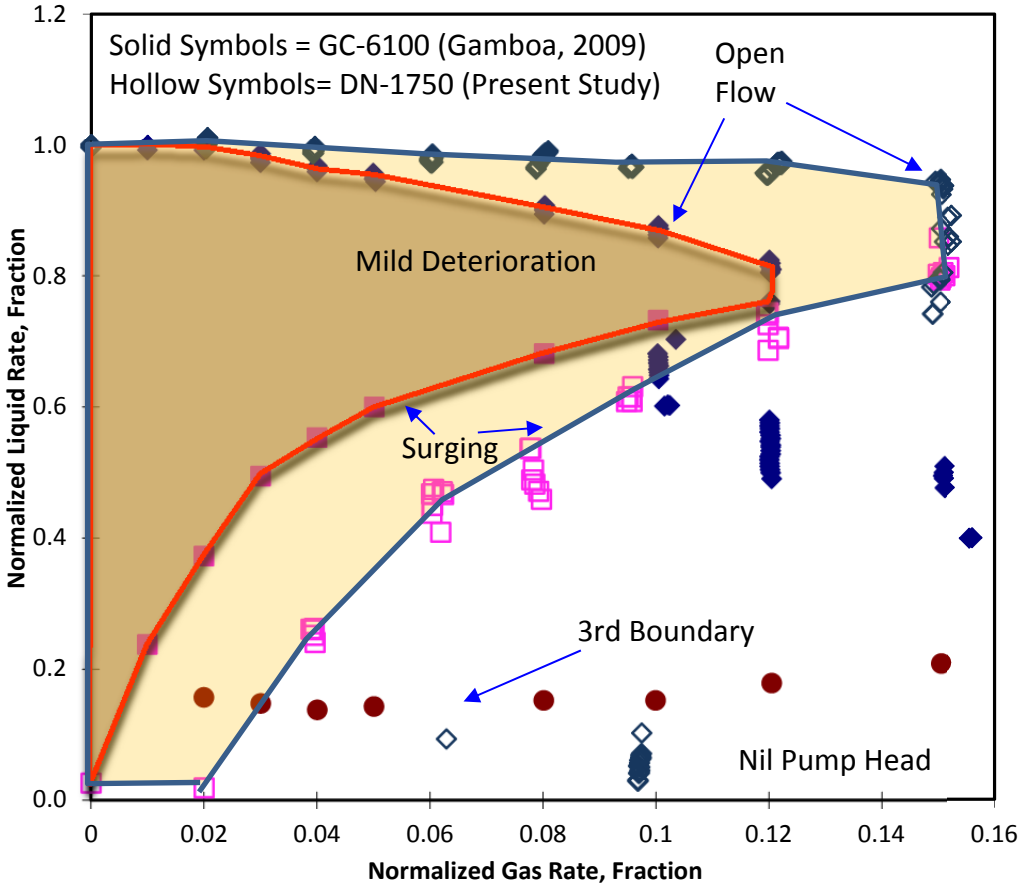

Fig. 14: Performance Map Comparison between GC-6100 and DN-1750

Conclusions

1. It is obvious that viscosity plays an important role in surging initiation. Increasing viscosity leads to earlier surging and the pump produces less pressure boosting. The mild deterioration region shrinks significantly when oil viscosity increases from 1 cP to 8.5 cP.
2. Almost every pressure increment curve follows the general pattern after the surging point. After the sudden drop, it starts to take a flat shape with the decrease of liquid flow rate. Then, it takes another dip which is called a secondary surging point.

3. In single-phase tests, the open-flow rate decreases with viscosity increase while the shut-in head is affected slightly with change of viscosity. This agrees with the Hydraulic Institute standards (1955).

Recommendations

1. Further studies are encouraged at higher viscosities to obtain different viscosity curves in the normalized liquid flow rate vs. normalized gas flow rate plot.
2. Bubble size effect and stage performance difference need to be investigated.
3. A more powerful booster pump is needed to produce the full performance curves at all ESP rotational speeds.
4. A cooling system and a temperature sensor are required to extend the achievable lowest oil temperature.
5. An online viscometer can be very helpful especially if oil is contaminated.
6. An oil temperature sensor at the oil flow meter and a gas temperature sensor at the gas flow meter will help better estimate the mixture temperature.

Nomenclature

BEP	Best efficiency point
BHP	Break horsepower
ESP	Electric submersible pump
f	Enhancement factor
GVF	Gas volumetric fraction
H	Pump head
N	Rotational speed
P	Pressure
Q	Flow rate
q_{gd}	Normalized gas flow rate
$q_{\max}$	Open-flow rate
q_g	Gas-volumetric flow rate
q_l	Liquid-volumetric flow rate
T	Temperature
VSD	Variable speed drive
γ	Fluid specific gravity
μ	Fluid viscosity
ρ	Fluid density

Acknowledgement

The authors would like to thank the Tulsa University Artificial Lift Projects (TUALP) members for their technical and financial support.

References

1. Hydraulic Institute 1955. *Determination of Pump Performance when Handling Viscous Liquid,* 10th Edition.
2. Stepanoff, A. J. 1957. *Centrifugal and Axial Flow Pump: Theory, Design, and Application,* second edition. New York, John Wiley & Sons.
3. Lea, J. and Bearden, J. 1982. Effect of Gaseous Fluids on Submersible Pump Performance. *SPE paper 9218 published in the JPT.*
4. Sutton, R and Farshad, F. 1990. Evaluation of Empirically Derived PVT Properties for Gulf of Mexico Crude Oils, *SPE Journal of Reservoir Engineering*, February: 79-86.
5. Rasmussen, K 1997. Calculation Methods for the Physical Properties of Air used in the Calibration of Microphones. Technical Report PL-11b, Department of Acoustic Technology, Technical University of Denmark, Denmark (May 1997).
6. Li, W. 2000. Effects of Viscosity of Fluids on Centrifugal Pump Performance and Flow Pattern in the Impeller. *International Journal of Heat and Fluid Flow* **21**: 207-212.
7. Duran, J. 2003. Pressure Effects on ESP Stages Air-Water Performance. MS thesis, The University of Tulsa, Tulsa, Oklahoma (2003).
8. Stachowiak, G. and Batchelor, A. 2005. *Engineering Tribology,* Third Edition.
9. Naseri, A., Nikazar, T. and Mousavi Dehghani, S. 2005. A Correlation Approach for Prediction of Crude Oil Viscosities. *Journal of Petroleum Science and Engineering* **47** (3-4): 163-174.
10. Gulich, J. 2007.*Centrifugal Pumps,* Second Edition. Springer.
11. Zapata, L. 2007. Rotational Speed Effects on ESP Two-Phase Performance. MS thesis, The University of Tulsa, Tulsa, Oklahoma (2007).
12. Takács, G. 2009. *Electrical Submersible Pumps Manual: Design, Operations, and Maintenance,* Gulf Professional Publishing.

13. Gamboa, J. 2009. Prediction of the Transition in Two-Phase Performance of an Electrical Submersible Pump. PhD dissertation, The University of Tulsa, Tulsa, Oklahoma (2009).
14. Solano, E. 2009. Viscous Effects on the Performance of Electric Submersible Pumps (ESP's). MS thesis, The University of Tulsa, Tulsa, Oklahoma (2009).
15. Trevisan, F. 2009. Modeling and Visualization of Air and Viscous Liquid in Electrical Submersible Pump. PhD dissertation, The University of Tulsa, Tulsa, Oklahoma (2009).
16. Prado, M. 2011. Production Engineering II. Lecture notes on ESPs, The University of Tulsa, Tulsa, Oklahoma.